Orientation of rod molecules in selective slits: a density functional theory

2008 J. Phys.: Condens. Matter 20 425221

(http://iopscience.iop.org/0953-8984/20/42/425221)

J. Phys.: Condens. Matter **20** (2008) 425221 (13pp) doi:10.1088/0953-8984/20/42/425221

Orientation of rod molecules in selective slits: a density functional theory

Xiaofei Xu, Dapeng Cao[1] and Wenchuan Wang

Division of Molecular and Materials Simulation, Key Lab for Nanomaterials, Ministry of Education, Beijing University of Chemical Technology, Beijing 100029, People's Republic of China

E-mail: caodp@mail.buct.edu.cn

Received 30 April 2008, in final form 26 August 2008
Published 30 September 2008
Online at stacks.iop.org/JPhysCM/20/425221

Abstract

A density functional theory (DFT) is used to investigate molecular orientation of rod fluids in selective slits. The DFT approach combines a modified fundamental measure theory (MFMT) for excluded-volume effect, the first-order thermodynamics perturbation theory for chain connectivity and the mean-field approximation for van der Waals (vdW) attraction. To study the molecular orientation, the intramolecular bonding orientation function is introduced into the DFT. First, we investigate the orientation of the surfactant-like rod molecule of AB_6 (i.e. ABBBBBB) in a nanoslit of $H = 20\sigma$, where the walls selectively adsorb segment 'A'. It is observed that, with the increase of the surface energy of the wall to head segment (i.e. 'A' segment) of the rod molecule, the rod molecules adsorbed on the wall present the perpendicular orientation gradually, and assemble into a smectic-A-like monolayer finally. In addition, we also explore the molecular orientation of the rods with both end segments preferring to the wall, i.e. AB_8A and AB_7A, in a nanoslit of $H = 10\sigma$. Interestingly, the AB_8A rod monolayer is compatible with either a smectic-A-like or a smectic-C-like organization, but AB_7A rod molecules exhibit the smectic-A-like organization. The orientation factor of the AB_7A rod molecule reaches 1, suggesting that AB_7A rod molecules self-assemble into an ordered structure with perfectly perpendicular orientation to the wall.

(Some figures in this article are in colour only in the electronic version)

1. Introduction

Self-assembled monolayers (SAM) are an ordered molecular assembly formed by the spontaneous adsorption of an active surfactant on a solid surface. Modular design of SAM allows for a broad range of applications, such as protective coating [1], friction/lubrication control [2], adhesion [3], filtering in biotechnology [4, 5] and fabricating large-area molecular junctions [6]. Various experiments and simulation results suggest that SAM undergoes an orientational and conformational change on increasing temperature [7]. This orientational behavior in thin SAM formed by rodlike molecules plays a central role in technological applications [8], especially as biosensors [9], smart elastomeric materials [10, 11] and nanoscale devices [12]. Many of these applications rely on the fact that the ordering of the rodlike molecules is affected by the physical or chemical properties of the surfaces. Accordingly, it is important to understand the thermodynamic and conformational properties of rod molecules in a confined space, like a slit, whose width reduces to a few molecular layers.

There are various studies on rodlike molecules in a confined space. In the study of Schmid *et al* [13], a tilting phase transition is predicted for systems comprising rodlike molecules which are grafted to a flat surface. They believed that the competition between bending elasticity and van der Waals attraction drives the transition. Cao *et al* [14] found that, in a hard slit, the chain length exhibits a more significant effect to determine the orientation, compared to the bulk packing fractions studied. By considering hard rod fluids confined in a slit of fixed width, van Roij *et al* [15] observed the continuous uniaxial–biaxial surface transition in the one-wall system and the first-order capillary condensation transition. By changing the affinity of the substrate toward the rodlike

[1] Author to whom any correspondence should be addressed.

molecule, de las Heras *et al* [16] observed the wetting behavior of the rodlike molecules on the substrate. Their results [17] also showed that the confinement of a nanoslit could lead to a rich phase behavior. Strong commensuration effect in the film with respect to wall separation causes an enhanced smectic ordering or frustrated smectic ordering. Micheletti *et al* [18] studied the effect of nanoconfinement on liquid-crystal polymer chains, and found that the anchoring conditions strongly affect chain structure, such as chain orientation and gyration radii. Gruhn *et al* [19] believed that the microscopic structure of thin molecular liquid-crystal films is a consequence of the competition between the orientation favored by the film–wall interaction potential and spatial constraints. In the regime of adsorption dominated by intermolecular interaction, Palermo *et al* [20] found a large and discontinuous change in orientation between the first and second adsorbed layers. Their results also showed that the structure of the first two adsorbed layers is entirely determined by the surface potential. Steuer *et al* [21] studied the phase behavior of liquid crystals confined in smooth walls and found that the confinement of flat walls forces the phase transition to be shifted, compared with the bulk. A homeotropic alignment is assembled with the increase of wall–particle interacting potential. However, an analytical and systematic study on the orientation of rodlike molecules induced by the wall potential is not available yet. Motivated by the wetting behavior of the rodlike molecules on the substrate from de las Heras *et al* [16], in this work we consider the molecular orientation of the rod molecules in the nanoslits, and explore the effect of surface energy of the wall to the segment on the molecular orientation of the rod molecules.

Currently, molecular simulations, integral-equation theory and density functional theory (DFT) are three main techniques to investigate the properties of the chain molecules, including flexible [22], semiflexible [23], rod–coil [24], star polymers [25] and rodlike molecules [23, 26, 27]. In the field of molecular simulations, the effects of confinement on rodlike fluid systems have been well studied. By modeling the polymeric molecule as a tangent hard sphere chain with a bending energy that can be used to tune the stiffness of the chain, Yethiraj *et al* [28] studied the isotropic–nematic phase transition in semiflexible polymer melts with 7 or 8 segments. Their results showed that an isotropic to nematic transition occurs at high pressures in the rod limit. Williamson *et al* [29] found that the flexibility of the chain has a large destabilizing effect on the nematic phase and postpones the isotropic–nematic transition. Using the hard ellipsoid model whose centroid cannot penetrate the surface while all other parts of the particle can, Allen [30] observed homeotropic surface alignment. This is in consistent with the findings of Cleaver *et al* [31] and Teixeira *et al* [32]. Subsequently, van Roij *et al* [15, 33] investigated the behavior of hard spherocylinders at a hard smooth wall and observed surface-induced wetting and planar ordering. These studies also showed that the planar arrangement is the natural state of the hard rod nematic phase in contact with a flat surface. Chrzanowska *et al* [30] and Cleaver *et al* [31, 34] used the hard Gaussian overlap model to investigate the confined symmetric and hybrid anchored films. Their results showed that the type of anchoring of hard rods at a substrate is determined by substrate penetrability. However, for the systems of high concentrations, molecular simulations are often computationally intensive and become invalid due to the restricted displacement of molecules.

DFT are capable of describing the structure of rodlike fluids near a solid surface and predicting the phase diagram, including translational ordered phases. In previous investigations, several DFT have been developed. Allen [30] presented that even the simplest density functional theory, i.e. the Onsager theory [35], can describe the structure of the surface layer under the influence of an external perturbation. Harnau *et al* [36, 37] studied hard rod fluids near geometrically structured substrates by DFT based on the Zwanzig model, where the rods are restricted to three mutually perpendicular orientations rather than a continuous range of orientations in space. Later, using the Zwanzig model together with the Rapini–Papoular surface free energy, they studied the phase behavior of a nematic liquid crystal in contact with a chemically and geometrically structured substrate [38, 39]. The combination of both chemical and geometrical surface pattern leads to much richer phase diagrams. Rickayzen and coworkers developed a DFT based on an expansion of density up to second order, together with the analogue of the Percus–Yevick and hyper-netted chain equations [40, 41]. They introduced a restricted orientation model in which the position of molecules is a continuous variable [33, 42], but its orientation can only take a discrete set of values. By increasing the number of allowed directions, Moradi *et al* studied the density profile and order parameter of a hard ellipsoidal fluid confined in a slit [43] and the surface anchoring of a confined liquid crystals [44]. By featuring the correct dimensional crossover and exact low density limit, Schmidt [45] constructed a DFT for the mixing/demixing of rods and spheres to extend the application in confined fluids.

Recently, a modified fundamental measure theory (MFMT)-based DFT has been developed and extensively applied to investigating properties of the different polymer systems, from the microstructure of flexible polymers [46–48], surface forces between polymer brushes [49], adsorption and phase behavior of polymer fluids in model pores [50–52] and phase transition in athermal solutions [53] to the self-assembly of polymers [54, 55]. All these investigations indicate that the MFMT-based DFT can excellently reproduce the microstructures and thermodynamic properties of polymeric fluids by comparison with these data from Monte Carlo simulations [56, 57]. In this work, the orientational and conformational properties of the rod molecules in a nanoslit would be studied by this MFMT-based DFT.

The rest of this work is organized as follows. First, we depict the models of the rod molecules and the nanoslit, and the interaction potentials between segments and between the segment and the wall. Second, we describe the MFMT-based DFT of the rod fluids from the Helmholtz energy functional, local density profiles, molecular orientation distribution function to numerical calculation details. Then, the calculated results of the orientation of the rod molecules in nanoslits are presented. Finally, some discussion is also addressed.

2. Models and potentials

2.1. Molecular models

In this work, the rodlike molecules are modeled as a tangentially connected hard sphere chain where the bond length is equal to the segmental diameter σ and the bond angle is fixed at $\theta_0 = \pi$. For the thermal system studied, the rod molecule contains two types of segments, where the two types of segments have the same size but different interaction energies: one is hydrophobic (denoted by 'A') and the other is hydrophilic (denoted by 'B'). To explore the local density profiles and molecular orientation of the rod molecule confined between two surfaces, the two surfaces are assumed to be hydrophobic. Therefore, the surfaces are selectively attractive to segments 'A', but repulsive to segments 'B'. The interaction between a segment and the surface is represented by a square well potential:

$$\varphi_{\mathrm{W}i}(z) = \begin{cases} \varepsilon_{\mathrm{W}i}, & 0 \leqslant z \leqslant \sigma \\ 0, & \text{otherwise} \end{cases} \tag{1}$$

where i equals A or B, the subscript W indicates the wall and $\varepsilon_{\mathrm{W}i}$ is the energy parameter. The intermolecular pair potential of segments is also represented by [46]

$$\varphi_{ij}(r) = \begin{cases} \infty, & r < \sigma \\ \varepsilon_{ij}, & \sigma \leqslant r \leqslant \gamma\sigma \\ 0, & r > \gamma\sigma \end{cases} \tag{2}$$

where i, j equals A or B, r is the distance between two segments. $\gamma\sigma$ is the square well width and ε_{ij} is the energy parameter. Throughout our work, the attractive width is fixed at $\gamma = 1.2$. The pair interaction between like segments (AA or BB) is always attractive and that between unlike segments is always repulsive. The unlike-pair interaction is fixed at $\varepsilon_{\mathrm{AB}} = 0.5k_{\mathrm{B}}T$. In order to mimic the behavior of hydrophobic effects, we assume that the attraction between AA segments ($\varepsilon_{\mathrm{AA}} = -1.0k_{\mathrm{B}}T$) is stronger than that between BB segments ($\varepsilon_{\mathrm{BB}} = -0.5k_{\mathrm{B}}T$), where the negative stands for attraction. The reduced temperature is defined as $T^* = k_{\mathrm{B}}T/\varepsilon_{\mathrm{AA}}$, where k is the Boltzmann constant and T is the absolute temperature. Throughout this work, the temperature is fixed at $T^* = 1.0$.

2.2. Bonding potential of rod molecules

The intramolecular potential for a tangentially connected hard sphere chain is represented by

$$V_{\mathrm{B}}(\boldsymbol{R}) = \sum_{i=1}^{M-1} V_{\mathrm{BL}}(|\boldsymbol{r}_{i+1} - \boldsymbol{r}_i|) + \sum_{i=2}^{M-1} V_{\mathrm{BA}}(\theta_{i-1,i,i+1}) \tag{3}$$

where the subscript B stands for the total bonding potential; subscript BL denotes the stretching potential related to the bond length; subscript BA represents the bending potential related to the bond angle. M is the number of segments for each chain, $\boldsymbol{R} = (\boldsymbol{r}_1, \boldsymbol{r}_2, \ldots, \boldsymbol{r}_M)$ representing the positions of all segments of the chain and $\theta_{i-1,i,i+1}$ is the bonding angle formed by three consecutive segments indexed by $i-1$, i and $i+1$. For the rod molecule studied here, the intramolecular Boltzmann factor satisfies [58]

$$\exp[-\beta V_{\mathrm{B}}(\boldsymbol{R})] = \prod_{i=1}^{M-1} \frac{\delta(|\boldsymbol{r}_{i+1} - \boldsymbol{r}_i| - \sigma)}{4\pi\sigma^2} \times \prod_{i=2}^{M-1} \frac{\delta^{(1)}(\theta_{i-1,i,i+1} - \pi)}{(1/2)} \tag{4}$$

where $\beta^{-1} = kT$, δ is the Dirac delta function and $\delta^{(1)}$ is the one-order generalized derivative of the Dirac delta function. The constant in equation (4) is determined from the normalization condition $(1/V)\int \exp[-\beta V_{\mathrm{B}}(\boldsymbol{R})]\,\mathrm{d}\boldsymbol{R} = 1$, where V is the system volume. Equation (4) indicates that the probability density of rod molecules with a configuration $\boldsymbol{R}$ is proportional to the Boltzmann factor $\exp(-\beta V_{\mathrm{B}}(\boldsymbol{R}))$.

3. Density functional theory

3.1. Helmholtz free energy functional

The grand potential and the Helmholtz free energy functional are related as

$$\Omega[\rho_{\mathrm{M}}(\boldsymbol{R})] = F[\rho_{\mathrm{M}}(\boldsymbol{R})] + \int [\psi_{\mathrm{M}}(\boldsymbol{R}) - \mu_{\mathrm{M}}]\rho_{\mathrm{M}}(\boldsymbol{R})\,\mathrm{d}\boldsymbol{R} \tag{5}$$

where $\mathrm{d}\boldsymbol{R} = \mathrm{d}\boldsymbol{r}_1\,\mathrm{d}\boldsymbol{r}_2\cdots\mathrm{d}\boldsymbol{r}_M$ is a differential volume, μ_{M} is the chemical potential and ψ_{M} is the external potential. For a rod consisting of M segments, the molecular density profile $\rho_{\mathrm{M}}(\boldsymbol{R})$ can be used to specify the segmental densities [22]:

$$\rho(\boldsymbol{r}) = \sum_{i=1}^{M} \rho_{si}(\boldsymbol{r}) = \sum_{i=1}^{M} \int \mathrm{d}\boldsymbol{R}\,\delta(\boldsymbol{r} - \boldsymbol{r}_i)\rho_{\mathrm{M}}(\boldsymbol{R}) \tag{6}$$

where $\rho(\boldsymbol{r})$ is the total segmental density and $\rho_{si}(\boldsymbol{r})$ is the local density of segment i. The Helmholtz energy functional $F[\rho_{\mathrm{M}}(\boldsymbol{R})]$ is conventionally expressed as an ideal contribution from a system of ideal chains (i.e. interacting only through bonding potentials) and an excess part taking into account these contributions from both inter- and intramolecular non-bonded interactions [57]

$$F[\rho_{\mathrm{M}}(\boldsymbol{R})] = F_{\mathrm{id}}[\rho_{\mathrm{M}}(\boldsymbol{R})] + F_{\mathrm{ex}}[\rho_{\mathrm{M}}(\boldsymbol{R})]. \tag{7}$$

The Helmholtz energy functional of ideal chains with a bonding potential is known exactly:

$$\beta F_{\mathrm{id}}[\rho_{\mathrm{M}}(\boldsymbol{R})] = \int \mathrm{d}\boldsymbol{R}\,\rho_{\mathrm{M}}(\boldsymbol{R})[\ln\rho_{\mathrm{M}}(\boldsymbol{R}) - 1] + \beta\int \mathrm{d}\boldsymbol{R}\,\rho_{\mathrm{M}}(\boldsymbol{R})V_{\mathrm{B}}(\boldsymbol{R}). \tag{8}$$

Different from a mixture of monatomic ideal gases, equation (8) includes the bonding potential that takes into account the direct chain connection [22]. For the systems considered in this work, the excess Helmholtz energy functional consists of contributions from the hard sphere repulsion, the van der Waals attractions, and the correlations due to chain connectivity [23]:

$$\beta F_{\mathrm{ex}}[\rho(\boldsymbol{r})] = \beta F_{\mathrm{ex}}^{\mathrm{hs}} + \beta F_{\mathrm{ex}}^{\mathrm{chain}} + \beta F_{\mathrm{ex}}^{\mathrm{att}}. \tag{9}$$

Following our previous work, the hard sphere part of the excess Helmholtz energy functional is represented by a modified fundamental measure theory [23, 59]:

$$\beta F_{\rm ex}^{\rm hs} = \int {\rm d}\boldsymbol{r}\Big\{-n_0\ln(1-n_3) + \frac{n_1 n_2 - \boldsymbol{n}_{\rm V1}\cdot\boldsymbol{n}_{\rm V2}}{1-n_3} + (n_2^3/3 - n_2\boldsymbol{n}_{\rm V2}\cdot\boldsymbol{n}_{\rm V2})\Big[\frac{\ln(1-n_3)}{12\pi n_3^2} + \frac{1}{12\pi n_3(1-n_3)^2}\Big]\Big\} \tag{10}$$

where $n_\alpha(\boldsymbol{r}), \alpha = 0, 1, 2, 3, {\rm V1}, {\rm V2}$ are scalar and vector weighted densities defined by Rosenfeld [60]. The excess Helmholtz energy functional due to the chain connectivity is given by a generalized first-order thermodynamics perturbation theory [23]:

$$\beta F_{\rm ex}^{\rm chain} = \frac{1-M}{M}\int {\rm d}\boldsymbol{r}\, n_0\xi \ln y^{\rm hs}(\sigma, n_\alpha) \tag{11}$$

where $\xi = 1-\boldsymbol{n}_{\rm V2}\cdot\boldsymbol{n}_{\rm V2}/n_2^2$ and $y^{\rm hs}(\sigma, n_\alpha)$ is the contact value of the cavity correlation function for hard sphere segments:

$$y^{\rm hs}(\sigma, n_\alpha) = \frac{1}{1-n_3} + \frac{n_2\xi\sigma}{4(1-n_3)^2} + \frac{n_2^2\xi\sigma}{72(1-n_3)^3}. \tag{12}$$

Finally, the excess Helmholtz energy functional due to square well attraction, $\beta F_{\rm ex}^{\rm att}$, is represented by a mean-field approximation [23]

$$\beta F_{\rm ex}^{\rm att} = \tfrac{1}{2}\int\int {\rm d}\boldsymbol{r}\,{\rm d}\boldsymbol{r}' \sum_{i,j={\rm A,B}} \rho_i(\boldsymbol{r})\rho_j(\boldsymbol{r}')\beta\varphi_{ij}(|\boldsymbol{r}-\boldsymbol{r}'|) \tag{13}$$

where $\varphi_{ij}(r)$ is a square well potential between segments.

3.2. Euler–Lagrange equation

Following variation principles, the molecular density $\rho_{\rm M}(\boldsymbol{R})$ can be solved from the stationary condition

$$\frac{\delta\Omega}{\delta\rho_{\rm M}(\boldsymbol{R})} = 0. \tag{14}$$

Namely, equations (5) and (14) yield the Euler–Lagrange equation [22]:

$$\rho_{\rm M}(\boldsymbol{R}) = \exp\left[\beta\mu_{\rm M} - \beta V_{\rm B}(\boldsymbol{R}) - \beta\sum_{i=1}^{M}\lambda_i(\boldsymbol{r}_i)\right] \tag{15}$$

where the self-consistent potential $\lambda_i(\boldsymbol{r}_i)$ includes the external potential $\varphi_i(\boldsymbol{r}_i)$ described in equation (1) and the derivative of the excess Helmholtz energy with respect to density profiles, given by

$$\lambda_i(\boldsymbol{r}_i) = \frac{\delta F_{\rm ex}}{\delta\rho(\boldsymbol{r}_i)} + \varphi_i(\boldsymbol{r}_i). \tag{16}$$

Equations (6), (15) and (16) yield the coupled integral equation:

$$\rho_{si}(\boldsymbol{r}) = \int {\rm d}\boldsymbol{R}\,\delta(\boldsymbol{r}-\boldsymbol{r}_i) \times \exp\left[\beta\mu_{\rm M} - \beta V_{\rm B}(\boldsymbol{R}) - \beta\sum_{j=1}^{M}\lambda_j(\boldsymbol{r}_j)\right] \tag{17}$$

or subsequently

$$\rho(\boldsymbol{r}) = \exp(\beta\mu_{\rm M})\int {\rm d}\boldsymbol{R}\sum_{i=1}^{M}\delta(\boldsymbol{r}-\boldsymbol{r}_i) \times \exp\left[-\beta V_{\rm B}(\boldsymbol{R}) - \beta\sum_{j=1}^{M}\lambda_j(\boldsymbol{r}_j)\right]. \tag{18}$$

3.3. Local density profiles

For the rod molecules in a nanoslit, the local density profiles of segments can be simplified as the following expression [23], because of the change of density only in the z direction:

$$\rho_{si}(z_i) = \frac{\exp(\beta\mu_{\rm M} - \beta\lambda_i(z_i))}{2\sigma}\int_{z_i-\sigma}^{z_i+\sigma} G_i^{\rm L}G_i^{\rm R}\,{\rm d}z_{i+1}, \quad 1\leqslant i\leqslant M \tag{19}$$

where the self-consistent potential $\lambda_i(z)$ is the one-dimensional form of equation (16). $G_i^{\rm L}$ and $G_i^{\rm R}$ are the left and right self-recursive functions, respectively, given by

$$G_i^{\rm L} = \begin{cases} 1, & i = 1 \\ \exp(-\beta\lambda_{i-1}(z_{i-1}))G_{i-1}^{\rm L}, & 1 < i \leqslant M \end{cases} \tag{20a}$$

$$G_i^{\rm R} = \begin{cases} \exp(-\beta\lambda_{i+1}(z_{i+1}))G_{i+1}^{\rm R}, & 1\leqslant i < M \\ 1, & i = M. \end{cases} \tag{20b}$$

The segmental coordinates $\{z_j | 1 \leqslant j \leqslant M\}$ of the rod molecules satisfies the relation

$$z_1 - z_2 = z_2 - z_3 = \cdots = z_i - z_{i+1} = \cdots = z_{M-1} - z_M.$$

The chemical potential can be calculated by [57]

$$\beta\mu_{\rm M} = \ln\rho_{\rm M} + M\beta\mu_{\rm M}^{\rm hs,bulk}(\rho_{\rm bulk}) + (1-M)\left[\ln y^{\rm hs,bulk}(\sigma) + \rho_{\rm bulk}\frac{\partial\ln y^{\rm hs,bulk}(\sigma)}{\partial\rho_{\rm bulk}}\right] + \sum_{i,j\in\{\rm A,B\}}(-4\pi/3)(\gamma^3-1)\varepsilon_{ij}^*\rho_{\rm bulk}x_ix_j\sigma^3 \tag{21}$$

where $\rho_{\rm bulk} = M\rho_{\rm M}$ is the total bulk density of all segments and $\mu^{\rm hs,bulk}$ is the excess chemical potential of hard spheres represented by the Carnahan–Starling equation of state. x_i is the molar fraction of segment i.

3.4. Orientation of the rod molecule

To obtain the local information on the molecular orientation of rods, we introduce the intramolecular distribution function (IMDF) into the present theory. The IMDF is described as [58, 61]

$$\rho_{i,i+1}(\boldsymbol{r},\boldsymbol{r}') = \int {\rm d}\boldsymbol{R}\,\delta(\boldsymbol{r}-\boldsymbol{r}_i)\delta(\boldsymbol{r}'-\boldsymbol{r}_{i+1})\rho_{\rm M}(\boldsymbol{R}). \tag{22}$$

For our systems studied, the IMDF can be derived analytically from equations (22) and (15) as

$$\rho_{i,i+1}(z,z') = \frac{\theta(\sigma-|z-z'|)}{2\sigma}\exp(\beta\mu_{\rm M} - \beta\lambda_i(z) - \beta\lambda_{i+1}(z'))G_{\rm L}^iG_{\rm R}^{i+1} \tag{23}$$

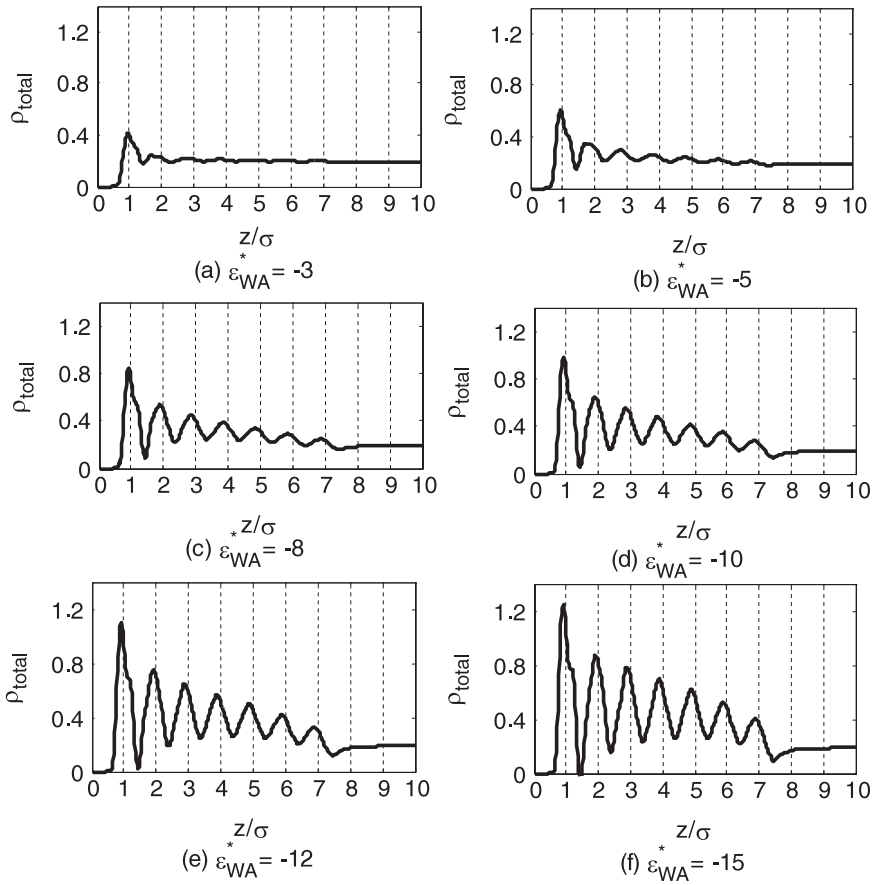

Figure 1. Total density profiles of the AB_6 rod molecule in a nanoslit of $H = 20\sigma$. From (a)–(f), the wall energies to segment 'A' are $\varepsilon^*_{WA} = -3, -5, -8, -10, -12, -15$, respectively (negative stands for attraction). The wall energy to segment 'B' is set to zero.

where $\theta(z)$ is the Heaviside step function. Then, the bonding orientation correlation function, $\cos\omega$, is evaluated from [61]

$$\langle\cos^2\omega\rangle = \frac{1}{M-1}\sum_{i=1}^{M-1}\frac{\int_{-1}^{1}\mathrm{d}y\,\rho_{i,i+1}(z-0.5y\sigma, z+0.5y\sigma)y^2}{\int_{-1}^{1}\mathrm{d}y\,\rho_{i,i+1}(z-0.5y\sigma, z+0.5y\sigma)} \tag{24}$$

where $y = \cos\omega$, ω is the polar angle between the z axis and the bond vector formed by two adjacent segments, and $\langle\,\rangle$ indicates the average of all bonding orientations of all configurations. Using the results of equation (23), we would get the value of $\langle\cos^2\omega\rangle$ by integrating with variable y in equation (24). Finally, the orientation distribution of the rod molecules can be defined as

$$s(z) = \frac{3\langle\cos^2\omega\rangle - 1}{2} \tag{25}$$

where z is the distance in the z direction. From the definition, we know that $s(z) = 1$ suggests that the orientation of the rod molecule is perpendicular to the surface, $s(z) = 0$ means random orientation of the rod molecule, while $s(z) = -0.5$ corresponds to the parallel orientation of the rod molecule to the surface.

3.5. Numerical calculations

In this work, the Picard iterative method is used to solve integral equations (19). The numerical integrations are performed using the Simpson method with a step size of $\Delta z = 0.02\sigma$. The iteration starts from the bulk density of the rodlike molecules. After a new density profile is obtained, we would combine the new density and the previous one in an appropriate prescription as a new input. The iterations terminated when the deviation between the old density and the new one is smaller than 10^{-5} at all the points.

4. Results and discussion

4.1. Surfactant-like rod molecules

To explore the orientation of the surfactant-like rod molecule in the nanoslit, the behavior of the AB_6 (i.e. ABBBBBB) rod molecule in a slit of pore size $H = 20\sigma$ was examined in this section. Since the head (i.e. segment 'A') of the surfactant-like rod molecule prefers the surface, the surfactant-like rod molecule may form the microscopic conformation perpendicular to the surface, which is closely dependent on the surface energy [20]. It is well known that a fluid of rods will exhibit ordered phase if it is compressed beyond a certain critical density [35]. Accordingly, in order to study the surfactant-like rod molecules in isotropic phase, the bulk packing fraction of the rod molecule was fixed at low packing fraction $\eta = 0.1$ [28, 29].

Figure 1 shows the total segmental density profiles of AB_6 rod molecules in the nanoslit of $H = 20\sigma$,

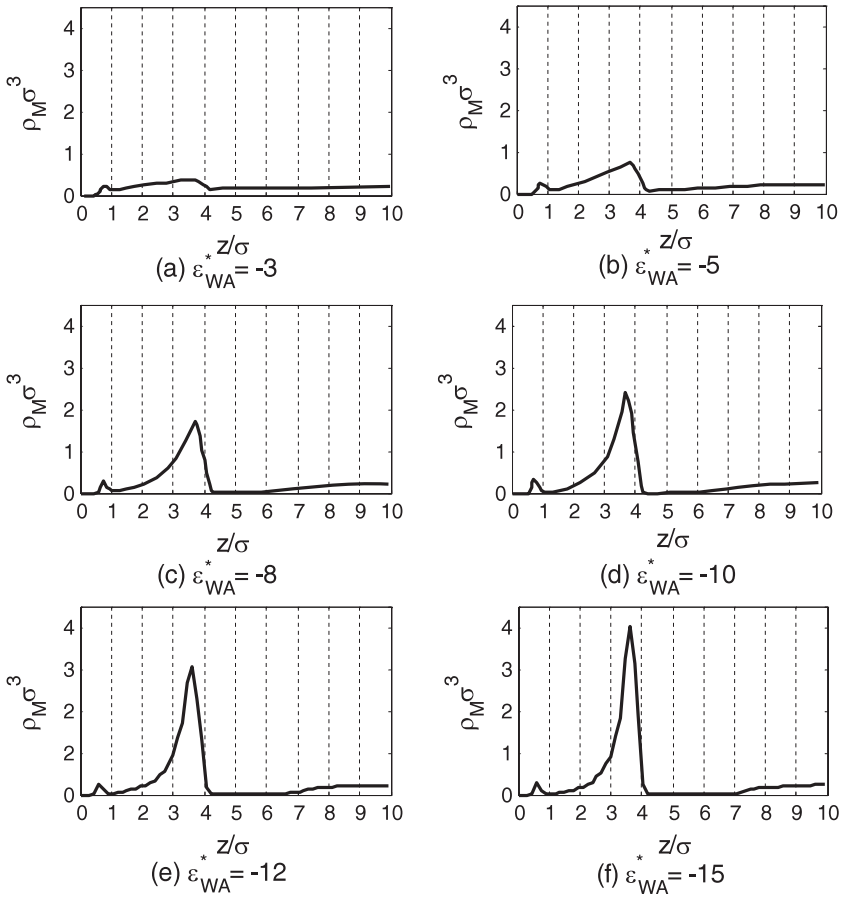

Figure 2. Molecular density profiles of the AB_6 rod molecule in a nanoslit of $H = 20\sigma$. Variable z represents the molecular centroid. All the conditions are the same as those in figure 1.

where the wall energies to segment 'A' are $\varepsilon^*_{WA} = -3, -5, -8, -10, -12, -15$, respectively, and the wall energy to segment 'B' is zero. The reduced energy parameters are defined as $\varepsilon^* = \varepsilon/k_BT$. It should be mentioned that all the density profiles in this work are represented by $\rho^* = \frac{N}{V}\sigma^3$ rather than by the normalized one $\rho^* = \frac{\rho_{Local}}{\rho_{Ave}}$. The reason is that the value of normalized density for segment 'A' is usually more than several times the value of segment 'B', which affects the clear observation. At $\varepsilon^*_{WA} = -3$, the density of the AB_6 rod molecule presents only a peak at $z = \sigma$. When the wall energy increases to $\varepsilon^*_{WA} = -5$, the density of the AB_6 rod molecule exhibits the second and third peaks besides the main peak at $z = \sigma$. With the increase of the wall energy, the main peak and other peaks in the density profiles become more and more prominent, and the layering order appears at $\varepsilon^*_{WA} = -15$.

Figure 2 shows the molecular density profiles of rods under the same conditions as figure 1. At $\varepsilon^*_{WA} = -3$, the rods are distributed uniformly in the silt. When the wall energies increase to $\varepsilon^*_{WA} = -5$, the molecular density exhibits a peak at $z = 3.5\sigma$. With the increase of the wall energy, the peak becomes higher and the density at other point gradually vanishes. It implies that a monolayer is gradually assembled at $z = 3.5\sigma$. Simultaneously, figure 3 shows the molecular orientation distribution of the AB_6 rod molecules in the nanoslit of $H = 20\sigma$, where all the conditions are the same as those in figure 1. It is found when the centroid of the AB_6 rod molecule is close to the wall, i.e. less than 2σ, the molecular orientation distribution function $s(z)$ is around -0.5, suggesting that the AB_6 rod molecules lie on the wall due to the confinement effect. With the distance between the centroid of the rod molecule and the wall increases to 4σ, the molecular orientation distribution presents a main peak, corresponding to the orientation perpendicular to the wall. The peak value is closely related to the wall energy. At $\varepsilon^*_{WA} = -3$, the peak value only reaches 0.5. That is to say, only a part of the rod molecules exhibit the orientation perpendicular to the wall. However, when the wall energy to segment 'A' increases more than $\varepsilon^*_{WA} = -8$, the peak value of the molecular orientation distribution of the rod molecule reaches 1 (denoted as type (I)). That is to say, in those cases, the rod molecules form a perpendicularly oriented layer to the wall. Interestingly, when the distance between the centroid of the rod molecule and the wall is beyond 4σ, the molecular orientation distribution function is equal to zero at $\varepsilon^*_{WA} = -3, -5$ and -8, suggesting the random distribution (also see type (III) in figure 4) of the rod molecules in these cases. However, the molecular orientation distribution function presents a valley (denoted as type (II)) at the position of $z = 7.5\sigma$ at $\varepsilon^*_{WA} = -12$ and -15. The valley suggests that the rod molecules are parallel to the wall. Actually, the rod molecules lie on the ordered layer formed by the rod molecules perpendicularly. The schematic diagrams of the conformation of the rod molecules

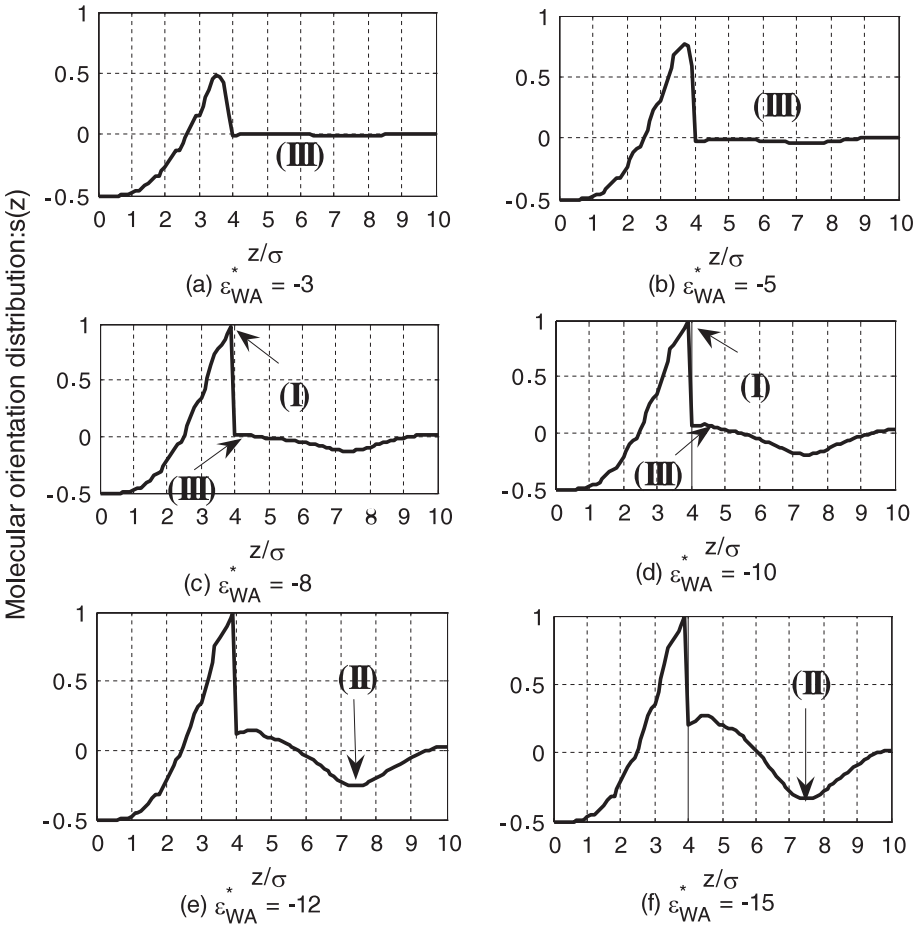

Figure 3. Molecular orientation distribution of the AB_6 rod molecule in the nanoslit of $H = 20\sigma$. All the conditions are the same as those in figure 1. Variable z in order function $s(z)$ represents the molecular centroid.

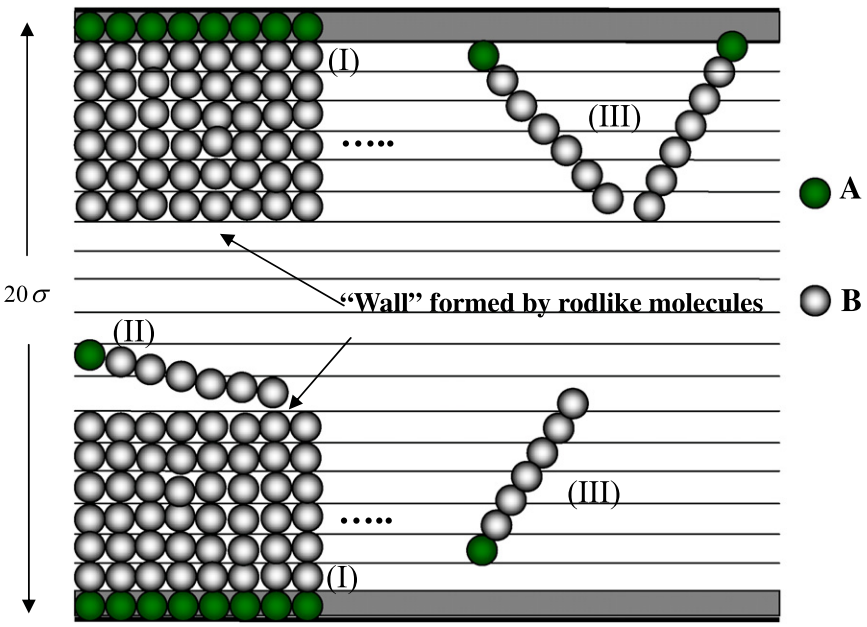

Figure 4. Schematic diagrams of the AB_6 rod molecule confined in a slit of $H = 20\sigma$. Type (I) shows that the rod molecules are perpendicular to the wall. Type (II) shows the configuration of the rods parallel to the slit wall because of the confinement of the 'wall' formed by type (I). Type (III) stands for random orientation of the rod molecule.

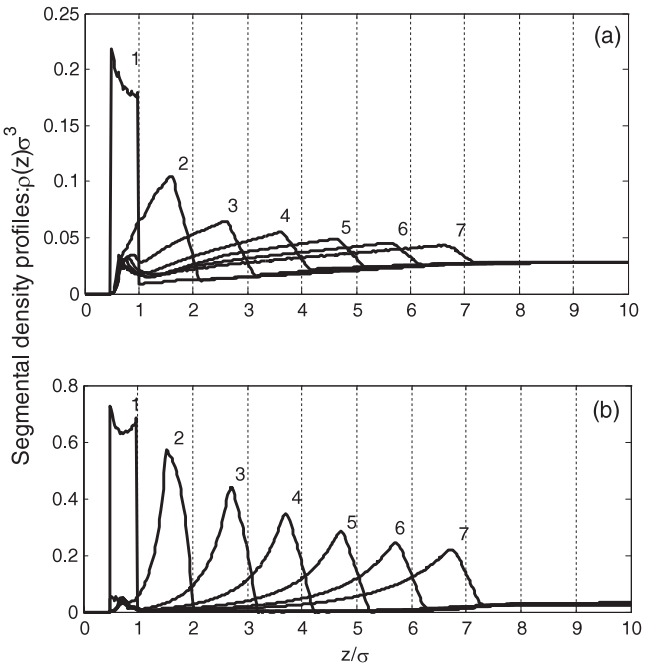

Figure 5. Local density profiles of individual segments of the AB_6 rod molecules in the nanoslit of $H = 20\sigma$. (a) $\varepsilon^*_{WA} = -3$ (b) $\varepsilon^*_{WA} = -10$. The wall energy to segment 'B' is set to zero.

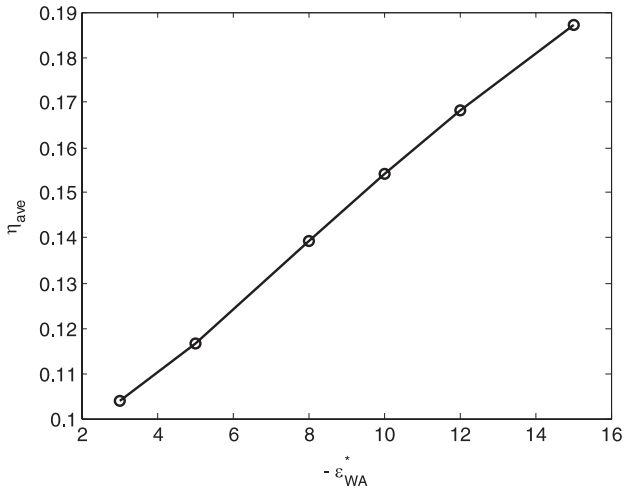

Figure 6. Average packing fraction profiles of AB_6 rod molecules in the nanoslit of $H = 20\sigma$. The wall energy to segment A varies as $\varepsilon^*_{WA} = -3, -5, -8, -10, -12, -15$, while ε^*_{WB} is set to zero. The average packing fraction is computed as $\eta_{ave} = \frac{\pi}{6}\rho_{ave}\sigma^3$, where $\rho_{ave} = \frac{1}{H}\int_0^H \rho(z)\,dz$ is the average density in the nanoslit.

corresponding to type (I)–(III) are shown in figure 4. The rod molecules of type (I) form a ordered layer when the centroid of the molecule is located at $z = 4\sigma$, and the rod molecules of type (II) have to adjust their conformation and exhibit the parallel orientation to the wall because of the formation of the perpendicularly oriented layer, also see type (I) in figure 4.

Besides the above molecular orientation distribution of the rod molecule, we can also use the local density profiles of segments to monitor the effect of the wall energy on molecular conformation. Figure 5 shows the local density profiles of the individual segments of the rod molecules between two surfaces, where the interactions between the head segment and the wall are $\varepsilon^*_{WA} = -3$ and -10, respectively. As is shown, the density variation is enormous between $\varepsilon^*_{WA} = -3$ and -10. The stronger the wall potential, the more rods would enter into the slit. In the statistics of the local density profile of segments, we only considered the centroid of segments. As a result, the more order the rod molecule oriented perpendicularly, the more prominent the peaks in the local density profile of segments. Therefore, the density variation of segments observed is attributed to the rodlike model made of spherical beads. For the system with low surface energy ($\varepsilon^*_{WA} = -3$), it can be observed that almost all the head segments are adsorbed on the surface, but 'B' segments present a random distribution. For the system with high surface energy ($\varepsilon^*_{WA} = -10$), however, we can find that, besides all head segments (i.e. segment 'A') are adsorbed on the surfaces, segments 'B' also exhibit an ordered distribution. The peak values of segments 'B' occur at the positions of $z = 1.6, 2.7, 3.8, 4.8, 5.8, 6.8\sigma$, respectively. That is to say, with the increase of the surface energy of the wall, the rod molecules adsorbed on the wall present a perpendicular orientation gradually, and form an ordered layer of smectic-A-like organization finally. This conclusion is consistent with the simulation result of Steuer *et al* [21], i.e. a homeotropic alignment is assembled gradually with the increase of wall–particle interacting potential. Our results show that the increasing of wall potential is responsible for this ordered layer.

To explain the effect of the packing induced by the wall energy on the orientational transition of the rod molecule, we present in figure 6 the average packing fraction of the rod molecules in the slit changing with the wall energy. Obviously, the stronger the wall energy, the higher is the packing fraction of the rod molecule. In particular, the packing fraction at $\varepsilon^*_{WA} = -3$ is about 0.103, which approximates the bulk one, while the packing fraction at $\varepsilon^*_{WA} = -15$ is about 0.188, which approaches two times the bulk one. Combined with the above analysis, it can be found that the formation of the ordered layer of the rod molecule at $\varepsilon^*_{WA} = -15$ benefits from the increase of the average packing fraction of the rod molecule induced by the strong wall energy. Accordingly, it is the wall energy that induces the disordered–ordered transition observed here. The schematic diagram of the wall energy-dependent orientation of the rod molecule is shown in figure 7.

4.2. Rod molecules with both end segments preferring to the wall

In section 4.1, we have investigated the dependence of molecular orientation of the surfactant-like rod molecules on the wall energy. In this section, we consider molecular orientation of the rods with both end segments preferring to the wall in a nanoslit of $H = 10\sigma$. Two types of rod molecules, i.e. AB_8A and AB_7A, were explored. To avoid two end segments of the AB_8A and AB_7A rod molecules adsorbing on one wall simultaneously, a slightly repulsive square well potential ($\varepsilon^*_{WB} = 2$, positive indicates repulsion) was used to represent the interaction between segment 'B' and the wall, which can avoid the parallel orientation of the rod molecule

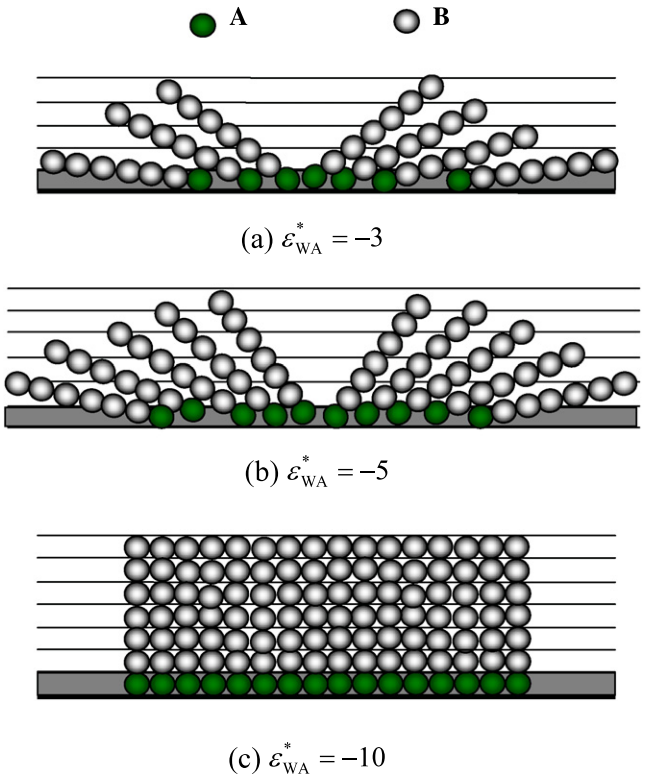

Figure 7. Schematic diagram of molecular orientation of the AB_6 rod molecule changing with the wall energies. (a) $\varepsilon^*_{WA} = -3$, (b) $\varepsilon^*_{WA} = -5$, (c) $\varepsilon^*_{WA} = -10$.

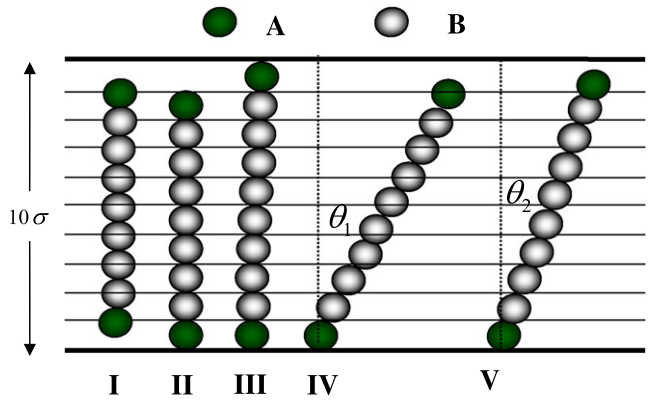

Figure 8. Schematic diagrams of the AB_7A and AB_8A rod molecules in the nanoslit of $H = 10\sigma$. Conformation (I) shows one of the perpendicular ways of the AB_7A rod, where two end segmental centroids are exactly at the boundary of the square well. Conformation (II) shows another perpendicular way of the AB_7A rod, where one end segment is wholly immersed in the well. Conformation (III) illustrates the perpendicular way of the AB_8A rod molecule, where two end segments are wholly immersed in the well. One of the end segmental centroids for conformation (IV) is exactly at the boundary of the well, while the other is wholly immersed in the well. Analogous to (IV), one of the end segmental centroids for conformation (V) is wholly immersed in the well, but the other end is partially immersed in the well. The angle formed by (V) with the normal line is less than that of (IV), i.e. $\theta_2 < \theta_1$.

to the wall. Therefore, when the AB_7A rod exhibits the normal orientation to the wall, the rod molecule may present two types of conformations, as shown as conformation (I) and (II) in figure 8. However, once the rod of AB_8A exhibits the normal orientation to the wall, the rod molecules just fill the separation between two walls, as shown as conformation (III) in figure 8. Actually, the AB_8A rod may also exhibit other configurations in the confinement, such as the conformations (IV) and (V) in figure 8. Once the AB_8A rod presents conformation (IV), we can calculate the corresponding orientation function value by

$$s_{IV} = 1.5 \times \cos^2\theta_1 - 0.5 = 1.5 \times \left(\frac{8.5\sigma}{9\sigma}\right)^2 - 0.5 = 0.837\,96. \tag{26}$$

For more information on the microscopic orientation of the rod molecules, we define the tilt angle θ of the rod orientation as $\theta = \arccos(|z_1 - z_M|/L)$, where L denotes the molecular length and z_1, z_M are the positions of two end segments in the z direction, respectively. For conformation (IV), we get $\theta_{IV} = \arccos(8.5/9) \approx 19°$. It implies that the monolayer is compatible with either a smectic-A-like or smectic-C-like organization.

The above analysis could also be confirmed by figure 9, which shows the molecular orientation distribution of the AB_8A rod in the slit of $H = 10\sigma$. Apparently, the orientation factor of the rod molecule does not reach 1.0, although the attractive energy of the wall to segment 'A' is large enough. It implies that the AB_8A rod monolayer is compatible with either a smectic-A or a smectic-C organization, i.e. it is difficult for the AB_8A rod to present conformation (III). Evidently, the average tilt angle of the AB_8A rod is about 10°, which confirms this analysis. The maximum value 0.88 in figure 9 is greater than s_{IV}, which means that the AB_8A rod may present conformation (V), i.e. the angle between the rod and the normal is less than that of conformation (IV). To get an insight into the microscopic information, figure 10 shows the local, total and molecular density profiles of the AB_8A rod at wall energy $\varepsilon^*_{WA} = -5, \varepsilon^*_{WB} = 2$. It can be found from figure 10(a) that all 'A' segments are adsorbed on the well of the wall, especially on the boundary of the wall. Figure 10(c) shows that all the molecular centroid is positioned around the center of the slit, which is in good agreement with the above analysis of molecular orientation.

Figure 11 shows the molecular orientation distributions of the AB_7A rod in the slit of $H = 10\sigma$ at two wall energies $\varepsilon^*_{WA} = -3, \varepsilon^*_{WB} = 2$ and $\varepsilon^*_{WA} = -5, \varepsilon^*_{WB} = 2$. Interestingly, when the centroid of the rod molecule is located at the center of the slit, the orientation factor of the rod molecule reaches 1, which means that the rod molecules present the normal orientation to the wall, i.e. the rod molecule exhibits the smectic-A-like organization in which the average tilt angle of the rod molecule is zero. Correspondingly, the main contribution comes from conformation (I) shown in figure 8. The above observation is entirely different from the behavior of the AB_8A rod molecule. To better explore the microstructure of the AB_7A rod molecules, figure 12 shows the local, total and molecular density profiles of the AB_7A rod molecule. Surprisingly, all peaks are distributed in the lattice positions of $z = n\sigma (n = 1–9)$ and all segments 'A' are distributed in the boundary of the well. Actually, the AB_7A rod molecules

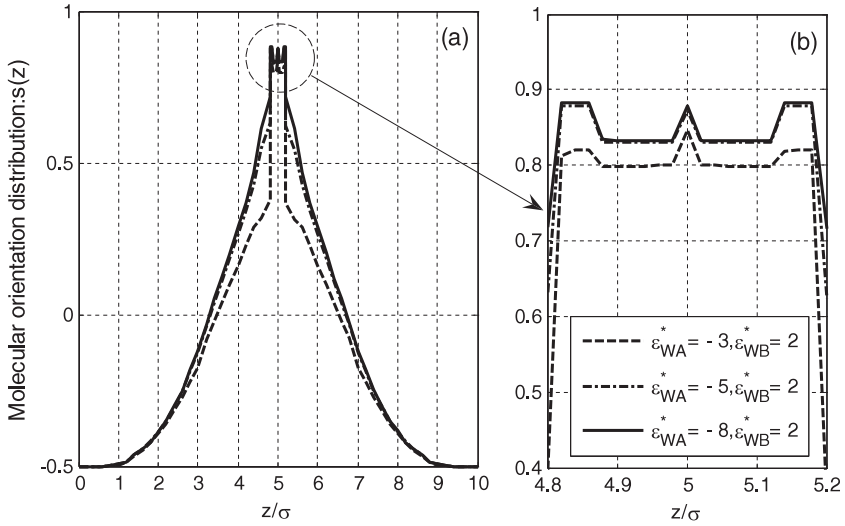

Figure 9. Molecular orientation distribution of the AB_8A rod molecule in the nanoslit of $H = 10\sigma$. The circular region in figure (a) is magnified in figure (b) for clear observation.

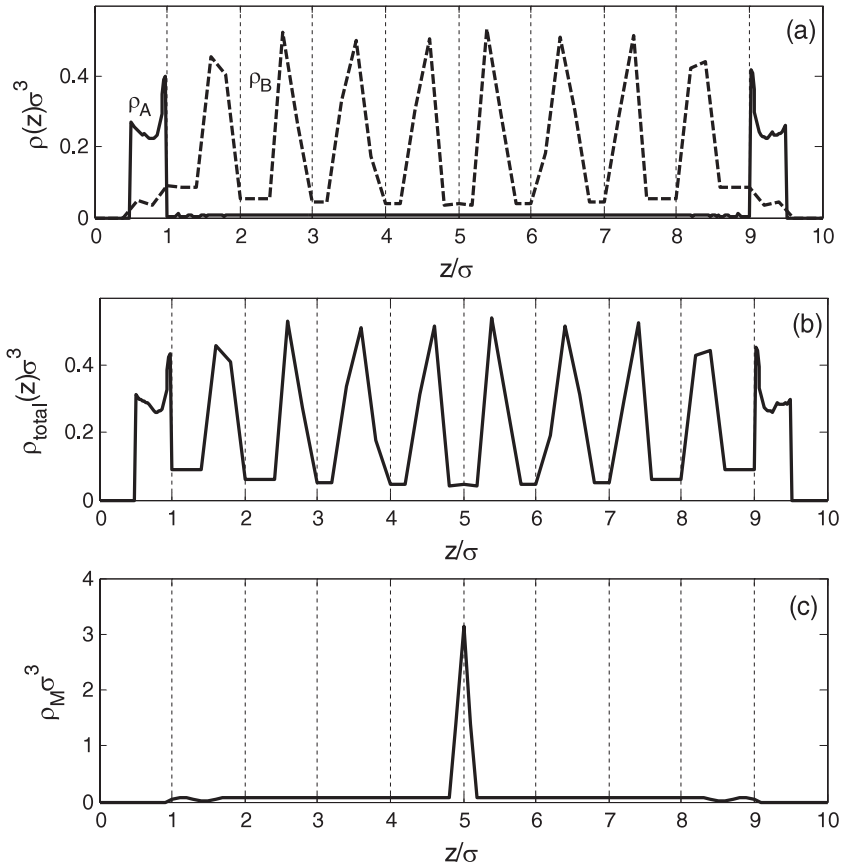

Figure 10. (a) Local, (b) total and (c) molecular density profiles of the AB_8A rod molecules in the nanoslit of $H = 10\sigma$ at $\varepsilon^*_{WA} = -5$, $\varepsilon^*_{WB} = 2$. Variable z in (c) represents the molecular centroid from the wall.

exhibit the smectic-A like organization, which is in excellent agreement with the analysis of molecular orientation. This analysis is confirmed by figure 12(c), where all the molecular centroids are positioned at the center of the slit. For illustration, the schematic diagram of the perfect structure of a smectic-A-like organization is shown in figure 13.

5. Conclusions

The molecular orientation of rod fluids in nanoslits has been investigated by a density functional theory, which combines a modified fundamental measure theory (MFMT) for excluded-volume effect, the first-order thermodynamics perturbation

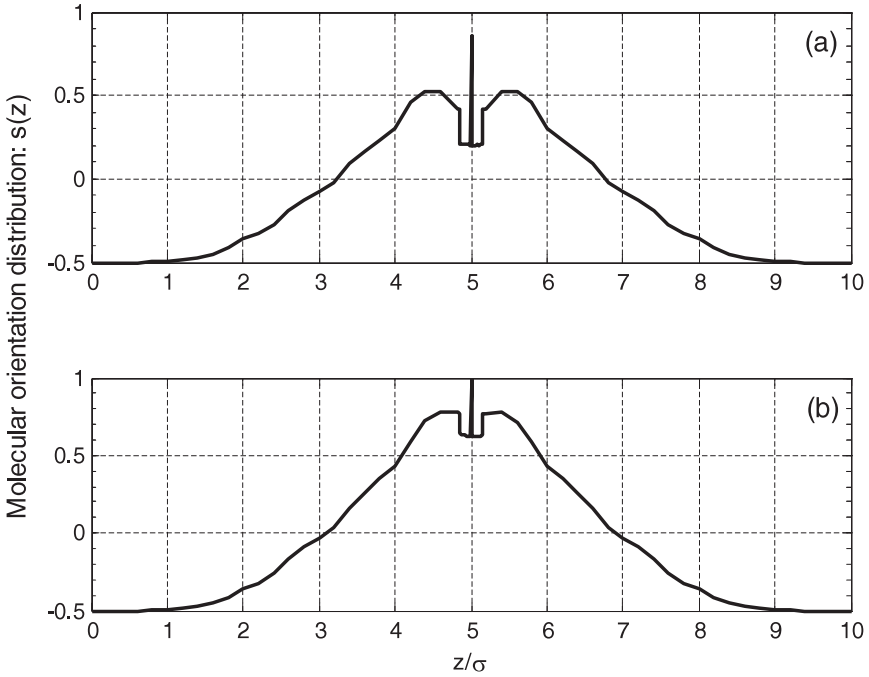

Figure 11. Molecular orientation distributions of the AB_7A rod molecule in the nanoslit of $H = 10\sigma$: (a) $\varepsilon^*_{WA} = -3$, $\varepsilon^*_{WB} = 2$, (b) $\varepsilon^*_{WA} = -5$, $\varepsilon^*_{WB} = 2$.

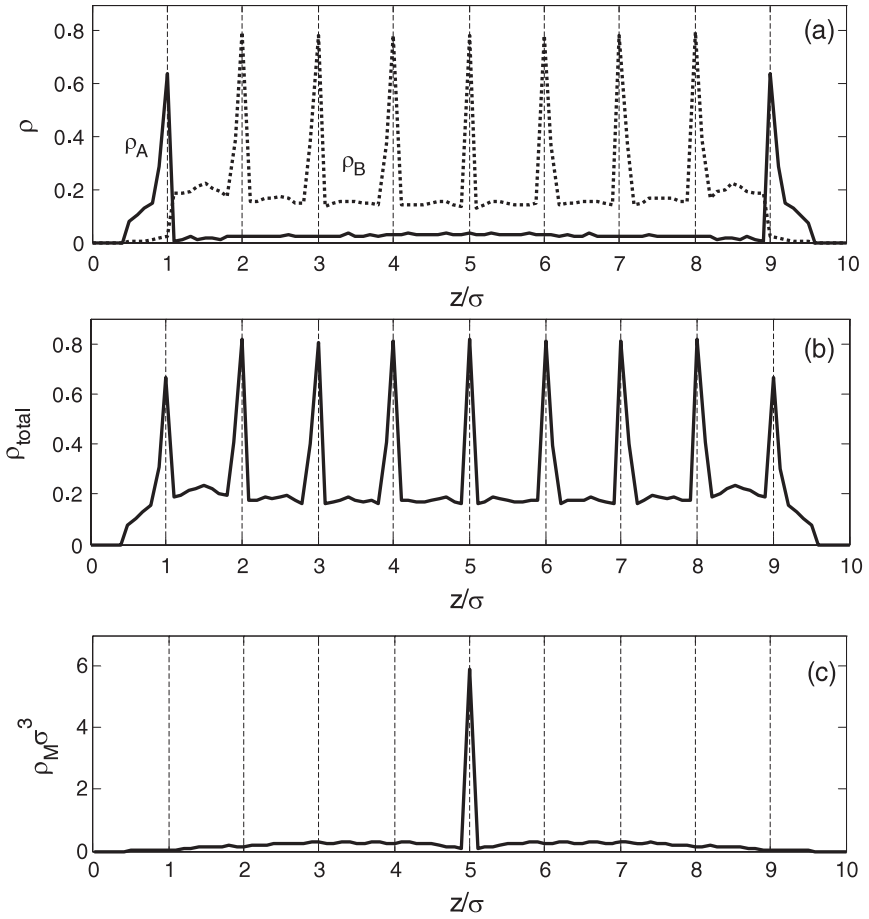

Figure 12. (a) Local, (b) total and (c) molecular density profiles of the AB_7A rod molecules in the nanoslit of $H = 10\sigma$ at $\varepsilon^*_{WA} = -5$, $\varepsilon^*_{WB} = 2$. Variable z in (c) represents the molecular centroid from the wall.

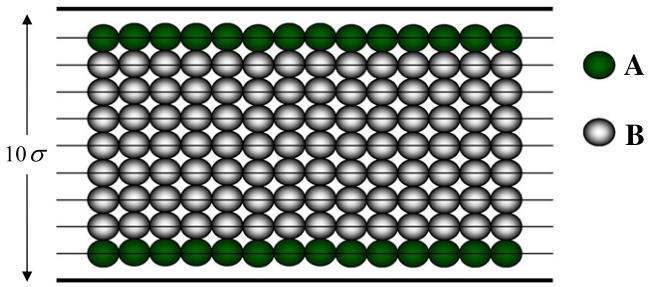

Figure 13. Schematic diagrams of the smectic-A-like organization formed by AB_7A in the slit of $H = 10\sigma$ at $\varepsilon^*_{WA} = -5$, $\varepsilon^*_{WB} = 2$.

theory for chain connectivity and the mean-field approximation for van der Waals attraction. For the purpose of investigating the molecular orientation of rod fluids, the intramolecular bond orientation function was introduced into the DFT approach. By studying the orientation of the surfactant-like rod molecule of AB_6 (which stands for ABBBBBB) in the nanoslit of $H = 20\sigma$, we observed that, with the increase of the attractive energy of the wall to segment 'A', the rod molecules adsorbed on the wall present the perpendicular orientation gradually and form an ordered layer of smectic-A-like organization finally. Furthermore, by exploring the molecular orientation of the rods with both end segments preferring to the wall, i.e. AB_8A and AB_7A, in the nanoslit of $H = 10\sigma$, we found that the AB_8A rod monolayer is compatible with either a smectic-A-like or smectic-C-like organization, but the AB_7A rod molecules exhibit the smectic-A-like organization. Interestingly, the orientation factor of the AB_7A rod molecule reaches 1, which means that the AB_7A rod molecules self-assemble into an ordered structure with the perfectly perpendicular orientation to the wall.

Acknowledgments

This work is supported by the National Natural Science Foundation of China (nos. 20776005 and 20736002), the Beijing Novel Program (no. 2006B17), The Program for New Century Excellent Talents in University (NCET-6-0095), and the 'Chemical Grid Program' and Excellent Talents Funding of BUCT.

References

[1] Scherer J, Vogt M R, Magnussen O M and Behm R J 1997 *Langmuir* **13** 7045
[2] Xiao X, Hu J, Charych D H and Salmeron M 1996 *Langmuir* **12** 235
[3] Kim S, Choi G Y, Ulman A and Fleischer C 1997 *Langmuir* **13** 6850
[4] Harder P, Grunze M, Dahint R, Whitesides G M and Laibinis P E 1998 *J. Phys. Chem.* B **102** 2426
[5] Wang R L C, Kreuzer H J and Grunze M 1997 *J. Phys. Chem.* B **101** 9767
[6] Akkerman H B, Blom P W M, De Leeuw D M and de Boer B 2006 *Nature* **441** 69
[7] Ruckenstein E and Li Z F 2005 *Adv. Colloid Interface Sci.* **113** 43
[8] Bahadur B 1990 *Liquid Crystal Application and Users* (Singapore: World Scientific)
[9] Gupta V K, Skaife J J, Dubrovsky T B and Abbott N L 1998 *Science* **279** 2077
[10] Finkelmann H, Nishikawa E, Pereira G G and Warner M 2001 *Phys. Rev. Lett.* **87** 015501
[11] Yu Y L, Nakano M and Ikeda T 2003 *Nature* **425** 145
[12] Hamley I W 2003 *Angew. Chem. Int. Ed. Engl.* **42** 1692
[13] Schmid F, Johannsmann D and Halperin A 1996 *J. Physique* II **6** 1331
[14] Cao D P, Cheng L S and Wang W C 2007 *Chin. Phys.* **16** 2296
[15] van Roij R, Dijkstra M and Evans R 2000 *J. Chem. Phys.* **117** 7689
[16] de las Heras D, Mederos L and Velasco E 2003 *Phys. Rev.* E **68** 031709
[17] de las Heras D, Velasco E and Mederos L 2005 *Phys. Rev. Lett.* **94** 017801
[18] Micheletti D, Muccioli L, Berardi R, Ricci M and Zannoni C 2005 *J. Chem. Phys.* **123** 224705
[19] Gruhn T and Schoen M 1997 *Phys. Rev.* E **55** 2861
[20] Palermo V, Biscarini F and Zannoni C 1998 *Phys. Rev.* E **57** 2519
[21] Steuer H, Hess S and Schoen M 2004 *Phys. Rev.* E **69** 031708
[22] Yu Y X and Wu J Z 2002 *J. Chem. Phys.* **117** 2368
[23] Cao D P and Wu J Z 2004 *J. Chem. Phys.* **121** 4210
[24] Cheng L S and Cao D P 2008 *J. Chem. Phys.* **128** 074902
[25] Malijevsky A, Bryk P and Sokolowski S 2005 *Phys. Rev.* E **72** 032801
[26] Bryk P, Bucior K, Sokolowski S and Zukocinski G 2005 *J. Phys. Chem.* B **109** 2977
[27] Cao D P and Wu J Z 2005 *Langmuir* **21** 9786
[28] Yethiraj A and Fynewever H 1998 *Mol. Phys.* **93** 693
[29] Williamson D C and Jackson G 1998 *J. Chem. Phys.* **108** 10294
[30] Allen M P 1999 *Mol. Phys.* **96** 1391
[31] Cleaver D J and Teixeira P I C 2001 *Chem. Phys. Lett.* **338** 1
[32] Teixeira P I C, Barmes F and Cleaver D J 2004 *J. Phys.: Condens. Matter* **16** S1969
[33] van Roij R, Dijkstra M and Evans R 2000 *Europhys. Lett.* **49** 350
[34] Chrzanowska A, Teixeira P I C, Ehrentraut H and Cleaver D J 2001 *J. Phys.: Condens. Matter* **13** 1
[35] Onsager L 1949 *Ann. New York Acad. Sci.* **51** 627
[36] Harnau L and Dietrich S 2002 *Phys. Rev.* E **66** 051702
[37] Harnau L, Penna F and Dietrich S 2004 *Phys. Rev.* E **70** 021505
[38] Harnau L, Kondrat S and Poniewierski A 2005 *Phys. Rev.* E **72** 011701
[39] Harnau L, Kondrat S and Poniewierski A 2007 *Phys. Rev.* E **76** 051701
[40] Kalpaxis P and Rickayzen G 1993 *Mol. Phys.* **80** 391
[41] Rickayzen G 1993 *Mol. Phys.* **80** 1093
[42] Dijkstra M, van Roij R and Evans R 2001 *Phys. Rev.* E **63** 051703
[43] Moradi M, Wheatley R J and Avazpour A 2005 *J. Phys.: Condens. Matter* **17** 5265
[44] Moradi M, Wheatley R J and Avazpour A 2005 *Phys. Rev.* E **72** 061706
[45] Schmidt M 2001 *Phys. Rev.* E **63** 050201
[46] Cao D P and Wu J Z 2005 *J. Chem. Phys.* **122** 194703
[47] Bryk P, Bucior K, Sokolowski S and Zukocinski G 2005 *J. Phys. Chem.* B **109** 2977
[48] Ye Z C, Cai J, Liu H L and Hu Y 2005 *J. Chem. Phys.* **123** 194902
[49] Cao D P and Wu J Z 2006 *Langmuir* **22** 2712
[50] Fu D 2006 *J. Chem. Phys.* **124** 164701
[51] Fu D and Li X S 2006 *J. Chem. Phys.* **125** 084716
[52] Li Z D, Cao D P and Wu J Z 2005 *J. Chem. Phys.* **122** 224701
[53] Jiang T and Wu J Z 2007 *J. Chem. Phys.* **127** 034902

[54] Cao D P, Zhu M H and Wang W C 2006 *J. Phys. Chem.* B **110** 21882
[55] Cheng L S and Cao D P 2007 *J. Phys. Chem.* B **111** 10775
[56] Cao D P, Jiang T and Wu J Z 2006 *J. Chem. Phys.* **124** 164904
[57] Cao D P and Wu J Z 2005 *Macromolecules* **38** 971
[58] Cao D P, Cheng L S and Wang W C 2007 *Chin. Phys.* **16** 2296
[59] Roth R, Evans R, Lang A and Kahl G 2002 *J. Phys.: Condens. Matter* **14** 12063
[60] Rosenfeld Y 1989 *Phys. Rev. Lett.* **63** 980
[61] Kierlki E and Rosinberg M L 1994 *J. Chem. Phys.* **100** 1716